



Account/Revue

Shedding light on the morphology of calcium oxalate monohydrate crystallites present in kidney biopsies in the case of hyperoxaluria



Dominique Bazin^{a, b, *}, Emmanuel Letavernier^{c, d}, Jean-Phillippe Haymann^{c, d}, Frederik Tielens^a, Alex Kellum^e, Michel Daudon^{c, d}

^a Sorbonne Universités, UPMC Univ Paris-6, CNRS, Collège de France, Laboratoire de chimie de la matière condensée de Paris, 11, place Marcelin-Berthelot, 75005 Paris, France

^b CNRS, LPS, Ba510, Université Paris-11, 91405 Orsay, France

^c Sorbonne Universités, UPMC University Paris-6, UMR S 1155, 75005 Paris, France

^d AP-HP, Hôpital Tenon, Explorations fonctionnelles multidisciplinaires, 75020 Paris, France

^e Department of Chemistry, Clemson University, Clemson, SC, USA

ARTICLE INFO

Article history:

Received 15 December 2015

Accepted 1 February 2016

Available online 9 March 2016

Keywords:

Hyperoxaluria

Kidney biopsy

SEM

FTIR

ABSTRACT

Hyperoxaluria corresponds to an excessive urinary excretion of oxalate anions. Hyperoxaluria may be associated with the presence of calcium oxalate monohydrate crystals in kidney tissue and in some cases may lead to renal failure. In this contribution, a set of ten kidney biopsies corresponding to patients affected by hyperoxaluria from various origins such as primary hyperoxaluria or gastrointestinal disease has been investigated through μ Fourier transform infrared (FTIR) spectroscopy and Field Emission scanning Electron Microscopy (FE-SEM). The complete set of results indicates that if the deposits are mainly constituted of calcium oxalate monohydrate, some of them are made of calcium phosphate apatite, an observation which underlines the use of physicochemical techniques instead of the classical staining procedures. Moreover, FE-SEM observations clearly show a diversity of the crystallite morphology. Such diversity suggests changes in the composition of the milieu along the nephron and different interactions between calcium oxalate crystals and ions or macromolecules such as osteopontin and/or Tamm–Horsfall protein for example. This approach may help the clinician to understand more deeply the biochemical parameters which determine the formation of calcium oxalate monohydrate crystallites in kidney tissue and define the corresponding etiology.

© 2016 Published by Elsevier Masson SAS on behalf of Académie des sciences. This is an open access article under the CC BY-NC-ND license (<http://creativecommons.org/licenses/by-nc-nd/4.0/>).

1. Introduction

Hyperoxaluria is a metabolic disorder that may lead in some cases to end-stage renal failure and is defined as the excessive urinary excretion of oxalate anions (greater than

50 mg/1.73 m² per 24 h) [1]. This disease is characterized by calcium oxalate deposition first in kidney tissue and in the case of severe decrease of the glomerular filtration rate in other tissues including bones, heart and vessels. Hyperoxaluria constitutes a multifactorial disease and among the different aetiologies related to hyperoxaluria, we can quote lethal genetic disorders of the glyoxylate metabolism (the primary hyperoxalurias) [2–8], gastrointestinal diseases including cancers, inflammatory bowel diseases and their

* Corresponding author. Sorbonne Universités, UPMC Univ Paris 06, CNRS, Collège de France, Laboratoire de Chimie de la Matière Condensée de Paris, 11 Place Marcelin Berthelot, 75005, Paris, France.

E-mail address: dominique.bazin@u-psud.fr (D. Bazin).

surgical therapy (secondary enteric hyperoxaluria [9]), cystic fibrosis, and overconsumption/production of oxalate or its precursors from exogenous sources. Bariatric surgery [10] and intestinal lymphangiectasia [11] may also lead to hyperoxaluria.

Primary hyperoxalurias (PHs) are related to inborn errors in the metabolism of glyoxylate and oxalate [2–8] and lead to recurrent nephrolithiasis, nephrocalcinosis, systemic oxalosis, and renal failure. Aside from combined liver/kidney transplantation, no curative treatment exists. Calcium oxalate monohydrate (COM) kidney stones related to PH exhibit a peculiar morphology at the macroscopic and the mesoscopic scale [12–14]. Crystallite morphologies play definitely a major role in the classification of kidney stones [13,15–17] and thus in the definition of their etiology.

This contribution is devoted to the characterization of ectopic calcifications present in kidney of patients suffering from severe hyperoxaluria [18–21]. If ectopic calcifications can be probed using a usual procedure based on staining, it is at the cost of limited information on their chemical nature [22–24]. To go beyond this drastic limitation, different techniques can be used [25–28]. Here, we have selected μ FTIR Transform Infra-Red (FTIR) spectroscopy [29–36] and Field Emission Scanning Electron Microscopy (FE-SEM) [37–39] in order to characterize the crystalline phases forming abnormal deposits and to describe precisely their topology and structure.

2. Material and methods

Ten kidney biopsies were investigated (Table 1). The biological samples came from Tenon Hospital (Paris, France). For tissue embedded in paraffin, the paraffin was chemically removed in order to improve the crystal detection under the microscope. Each sample was only named with a study number, without indication of the name of the patient or potential identification data.

2.1. μ FTIR microspectroscopy

The starting point of this investigation was given by μ FTIR data in order to localize and determine the chemical nature of the pathological deposits present in kidney biopsy [39]. To fulfill IR reflexion, kidney biopsies were deposited on low-e microscope slides (MirrIR, Kevley

Technologies, Tienta Sciences, Indianapolis). FTIR hyper-spectral images were recorded with a Spectrum Spotlight 300 FTIR imaging system (Perkin Elmer Life Sciences, France), with a spatial resolution of 6.25 μm and a spectral resolution of 8 cm^{-1} . Each spectral image, covering a substantial part of the biopsy, consisted of about 30 000 spectra.

IR microspectroscopy was also performed on an IN10MX microscope (Thermo Scientific) for recording large maps. All spectra were collected in ultrafast mode using a 50 μm \times 50 μm aperture. The spectra were collected in the 4000–800 cm^{-1} mid-IR range at a resolution of 16 cm^{-1} with one spectrum per pixel. Data analysis of IR spectra and chemical images was performed using OMNIC software (Thermo Scientific).

2.2. Field Emission Scanning Electron Microscopy

A Zeiss SUPRA55-VP SEM was used for observation of the microstructure [37,39]. This field-emission “gun” microscope (FE-SEM) operates at 0.5–30 kV. High-resolution observations were obtained by using 2 secondary electron detectors: an in-lens SE detector and an Everhart-Thornley SE detector. Measurements were taken at low voltage (between 0.5 and 2 kV) without the usual deposits of carbon at the surface of the sample. Energy Dispersive X-ray (EDX) experiments can also be performed. In order to perform Ca cartography, the FE-SEM was operated at 12 kV.

3. Results and discussion

Quite recently, calcium oxalate compounds have been the subject of different publications [40–44] which have been dedicated to the insertion of heavy elements in their structure [45] or to their synthesis [46]. From a chemical point of view, the synthesis of amorphous COM can be considered a breakthrough in the chemistry of calcium oxalate compounds [47]. Among the different investigations we can quote the study of the adhesion and internalization between African green monkey kidney epithelial cells (before and after oxidative damage by hydrogen peroxide) and COM nanocrystals [48] or the internalization into MDCK renal tubular cells of COM crystals by endolysosomes [49]. As underlined by H. Shiraga et al. [50], although normal urine is frequently supersaturated with respect to calcium oxalate, most humans do not form stones. Inhibitors are among the multiple factors that may influence the complex process of urinary stone formation.

Regarding diseases related to calcium oxalate crystal deposition that lead to a significant loss of the kidney function, prevalent attention has been paid to hyperoxaluria. Although numerous excellent investigations exist [9,10,51–53], little attention has been paid to the crystallite morphology of COM ectopic calcification. This justifies the efforts undertaken here to describe the topology of these abnormal mineral deposits as well as their spatial repartition. In order to do so, the first step is to localize the COM deposits in the kidney biopsy.

Table 1
Etiology corresponding to the selected kidney biopsies.

Sample	Etiology
B274	Primary hyperoxaluria diagnosed after kidney transplantation
B279	Excessive consumption of rhubarb
B292	Ethylene glycol intoxication
B305	Nephrocalcinosis after kidney transplantation
B317	Nephrocalcinosis after kidney transplantation
B329	Primary hyperoxaluria
B364	Cystic fibrosis
B379	Bariatric surgery
B380	Stomach cancer
B386	Nephrocalcinosis after kidney transplantation

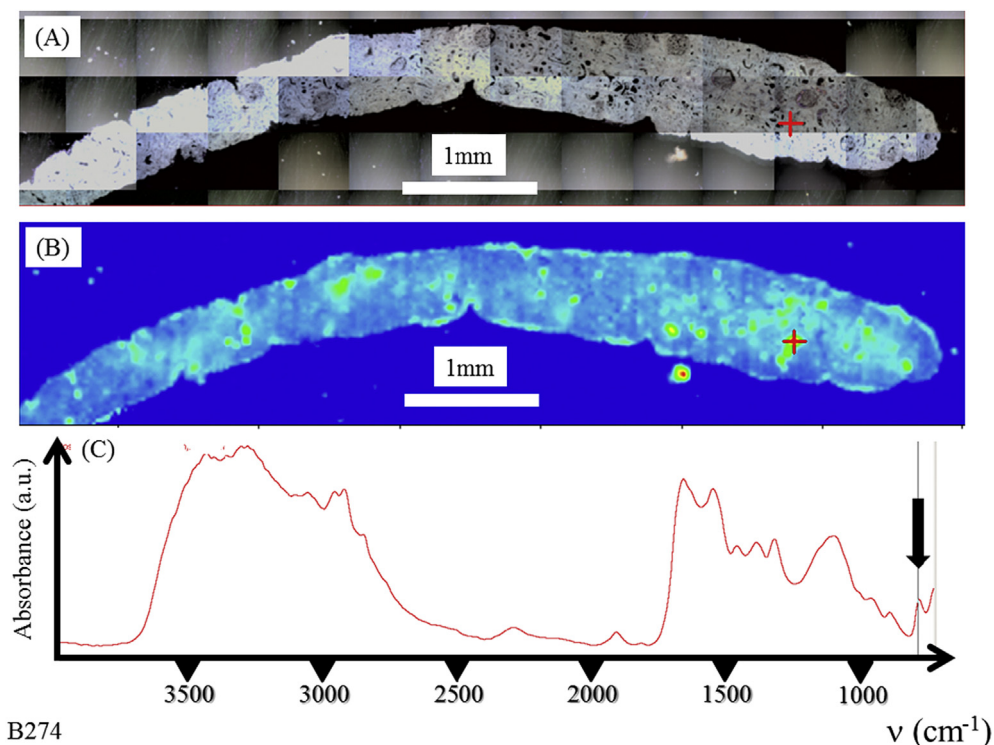


Fig. 1. Graft kidney in a patient suffering from primary hyperoxaluria (B274). (A) Optical photography, and (B) Spatial distribution of COM deposits in the biopsy as given by the intensity of the infrared spectrum (C) at 780 cm^{-1} .

μ FTIR is an invaluable tool to probe pathological calcifications present in kidney [54–65]. Fig. 1 shows an example of FTIR data which can be gathered on a kidney biopsy (Fig. 1A). The precise identification of pathological deposits is straightforward through the position of typical IR absorption bands. In fact, a typical tissue spectrum has two primary features due to proteins, the amide I ($1600\text{--}1700\text{ cm}^{-1}$) and amide II ($1500\text{--}1560\text{ cm}^{-1}$) bands, which arise primarily from the C–O and C–N stretching vibrations of the peptide backbone, respectively [30,66,67]. Far from these biological contributions, it is generally the IR absorption band positioned at 780 cm^{-1} which is selected to obtain the spatial distribution of COM crystallites. This typical band corresponds to the $\delta(\text{O}=\text{C}=\text{O})$ vibration.

As evidenced in Fig. 2, even small biopsy samples may be analyzed through this approach and provide useful information (Fig. 2D and E). At this point it is worth underlining that μ FTIR is capable of identifying different kinds of chemical phases in the same biopsy. It is the case of the biopsy B317 for which COM (Fig. 2G and H) as well as calcium phosphate apatite (Fig. 2I and J) are present.

The second step of this investigation is given by observations at different magnifications through last generation FE-SEM. On the very same sample on which FTIR measurements have been performed, FE-SEM offers the opportunity to describe at the submicrometer scale the topology of mineral deposits present in biopsy. Such a combined approach which mixed chemical identification

(through FTIR microspectroscopy) and topology description (through FE-SEM) both at the cellular level is exemplified in Fig. 3. Details regarding the crystallite morphology can be obtained through observations at high magnification.

Similar data have been gathered for the different kidney biopsies selected in this study as shown in Fig. 4 (for the biopsy B292) and Fig. 5 (for the biopsy B317). As previously underlined, all the deposits are not made of COM for the biopsy B317 and the red star in Fig. 5 indicate the location of a deposit made of calcium phosphate apatite. Of notice is that the precise description of the crystallite morphology can be obtained even for small kidney biopsies.

Even if the number of samples is limited, the complete set of observations through FE-SEM indicates that COM deposits may exist with very different topologies whatever the etiology of hyperoxaluria is. This diversity is clearly visible in Fig. 3 (B274) which corresponds to genetic hyperoxaluria, in Fig. 4 (B292) which corresponds to hyperoxaluria related to the consumption of ethylene glycol or in Fig. 5 (B317) which corresponds to COM and carapatite deposits in a grafted kidney. Another cause of hyperoxaluria is bariatric surgery, as shown in Fig. 6, where COM crystallites may form poorly organized platelets in tubular lumens. In other cases, some ectopic COM calcifications are made of an agglomeration of COM platelets with a concentric distribution (Fig. 7). Such diversity may be, at least in part, related to the location of deposits, most of them being observed in the lumen of tubules while

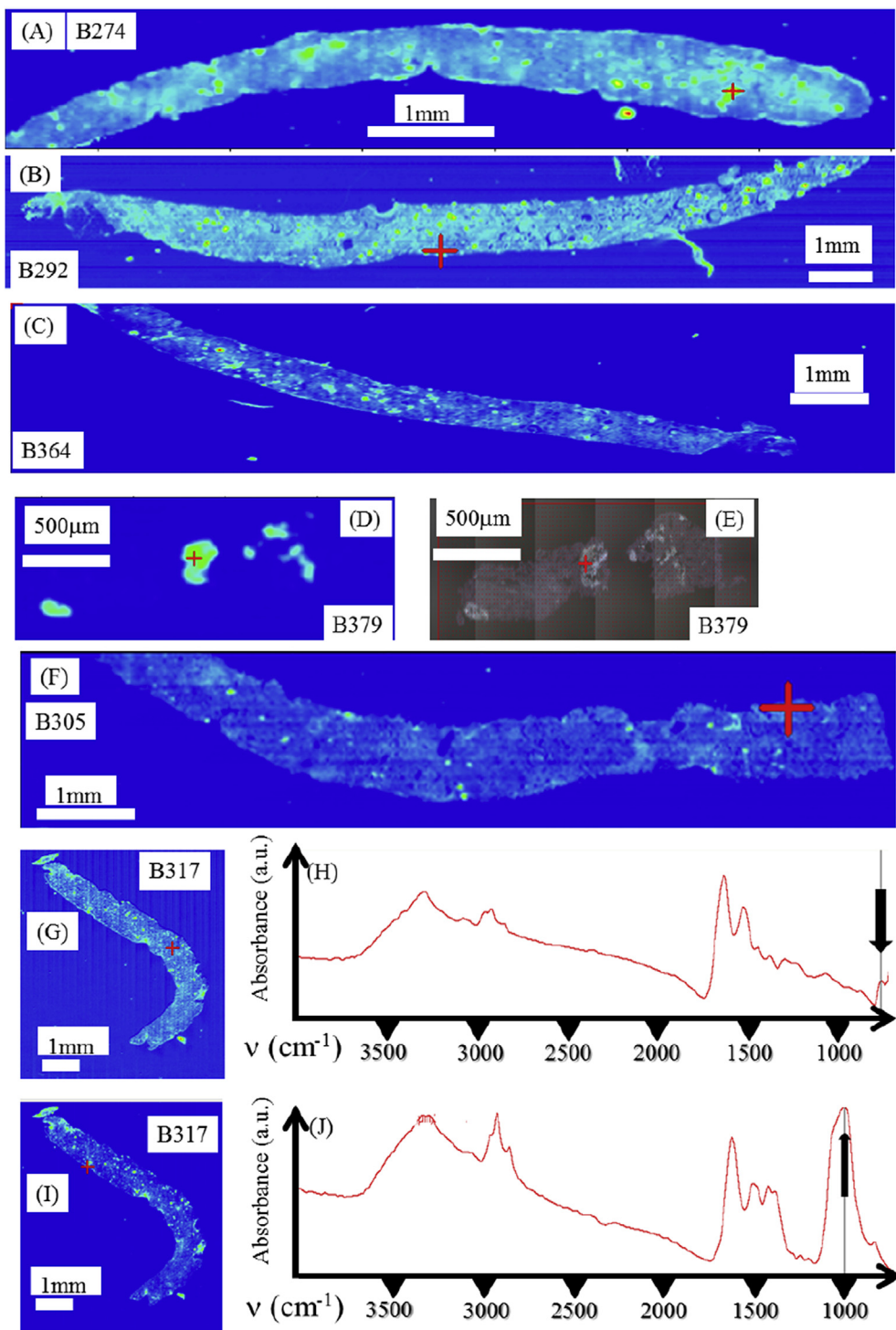


Fig. 2. (A) Spatial distribution of COM deposits as given by the intensity of the infrared spectrum at 780 cm^{-1} for different biopsies. (A) Primary hyperoxaluria (B274); (B) Ethylene glycol poisoning (B292); (C) Cystic fibrosis (B364); (D) Bariatric surgery (B379), (F) and (G) Nephrocalcinosis after kidney transplantation (B305 and B317); (H,J) infrared spectra of biopsy B317: (H) Infrared spectrum of COM deposit located by the red cross in figure (G), (J) Infrared spectrum of calcium phosphate present in some parts of the biopsy as a mixture of carapatite (CA) and amorphous carbonated calcium phosphate (ACCP) deposits located by the red cross in figure (I); (I) Spatial distribution of CA + ACCP deposits as given by the intensity of the infrared spectrum at 1030 cm^{-1} for biopsy B317.

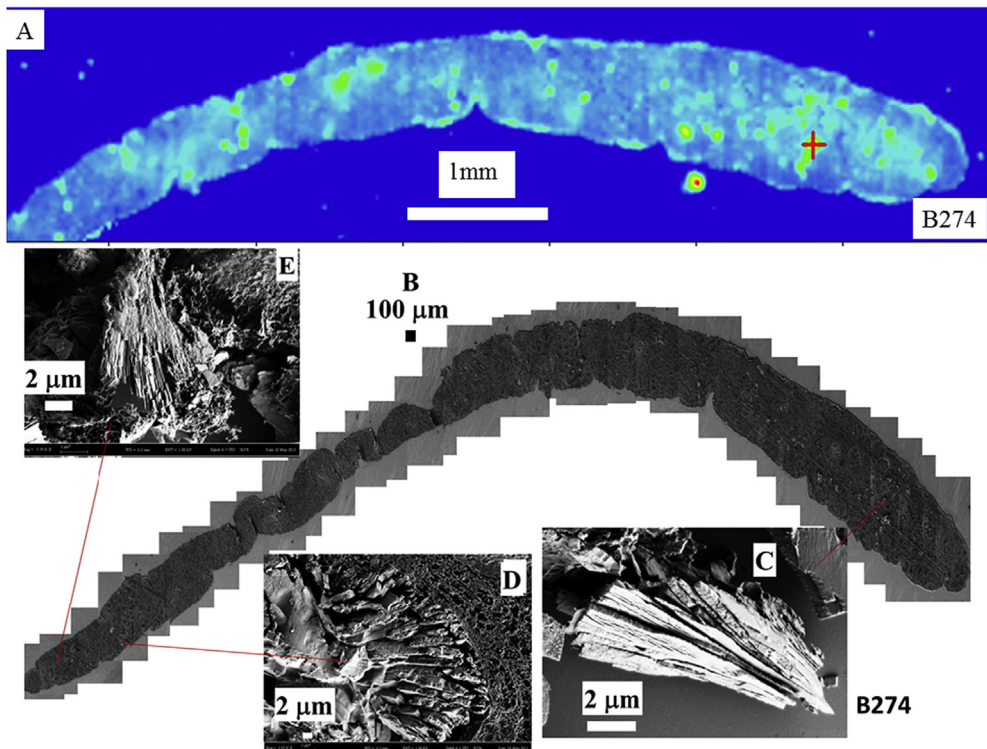


Fig. 3. (A) Spatial distribution of COM deposits in biopsy B274 as given by the intensity of the infrared spectrum at 780 cm^{-1} and the topology of the different abnormal deposits. (B) Topology of the different abnormal deposits for the biopsy B274. (C, E) Radial agglomeration of COM platelets and (D) agglomeration of platelets.

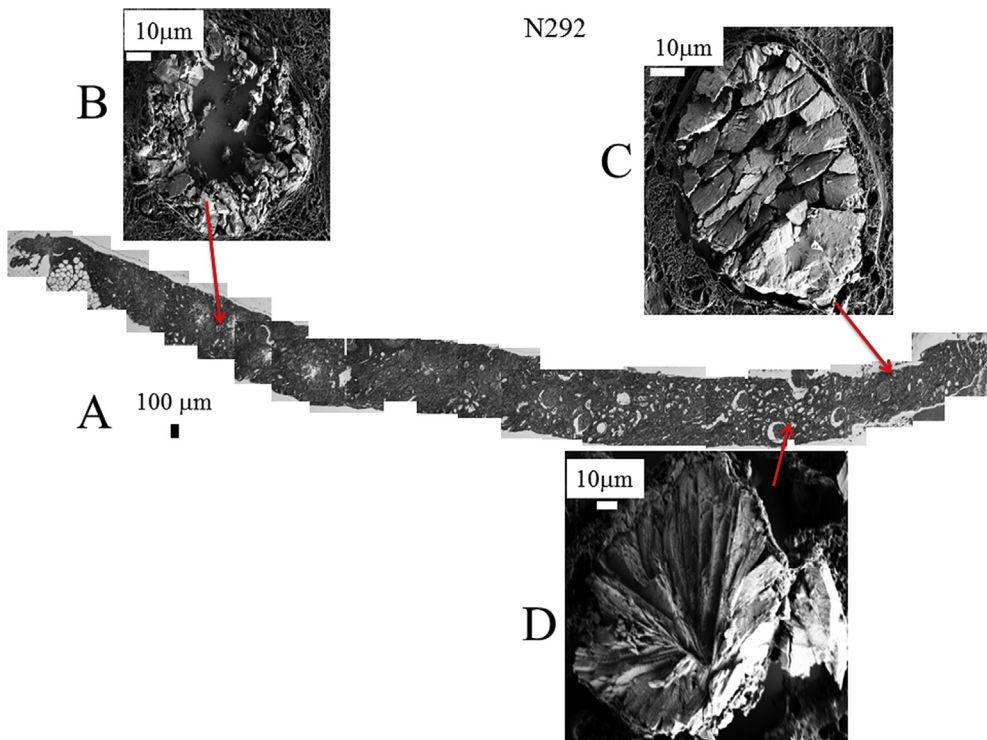


Fig. 4. A: Topology of the different abnormal deposits in the biopsy B292. Agglomeration of "large" crystallites is observed in the lumen of tubules (C) while agglomeration of "small" crystallites is located in the tubular cells (B). (D) Radial agglomeration of platelets.

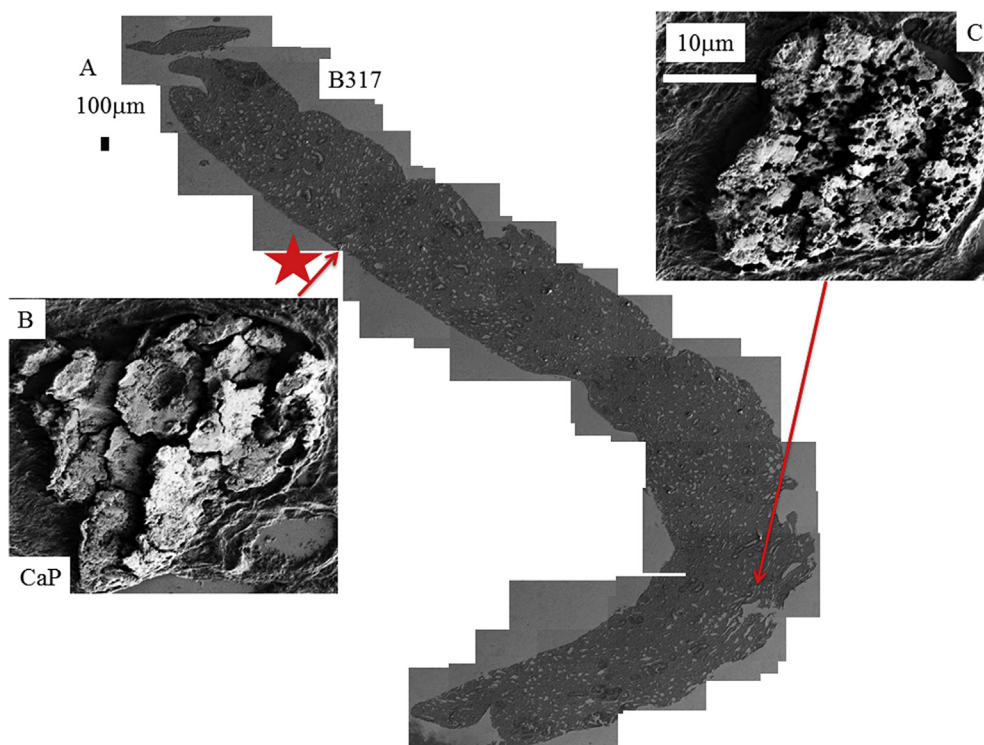


Fig. 5. A: Topology of the different abnormal deposits for the biopsy B317. B: The red star corresponds to the deposit of CA. C: Presence of numerous holes on the surface of a compact agglomeration of crystallites.

others seem to be located in the tubular cells (Fig. 4). The size of crystallites seems to be small for deposits within cells by comparison to deposits accumulated in the tubular lumen where a radiating organization of the crystallites is

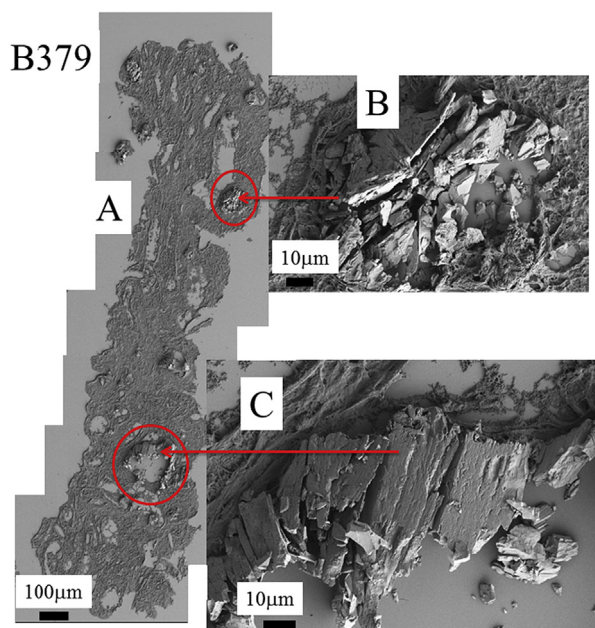


Fig. 6. A: Topology of the different abnormal deposits at different magnifications for the biopsy B379. B and C agglomeration of “large” and “small” crystallites.

often encountered (Figs. 5 and 8). In the case of biopsy B274, very different topologies may be observed (Fig. 9). Another cause for the diversity in the morphology of the deposits is the chemical composition. Fig. 5 shows various images of deposits of biopsy B317; Fig. 5C corresponds to calcium oxalate deposits while Fig. 5B corresponds to calcium phosphate plugs in the tubular lumen.

From a chemical point of view, it is well known that adsorption of molecules at the crystal surface may modify the crystal's morphology [68–71]. In Fig. 10, typical synthetic COM crystals are shown for which the crystallographic face has been indicated through their miller indices [72]. Adsorption of some molecules (here peptides) leads to the formation of a “smooth” apical tip. Such modification of the morphology is well known, adsorption of molecules is preferentially observed on undercoordinated atoms of corners, ridges, or faces leading to their eventual reconstruction and formation of new faces which will determine the final exposure of these new faces and thus the crystallite's morphology in the native solution. Note that some anionic surfactants, however, not only changed the crystal shape, but also induced the formation of metastable calcium oxalate dihydrate (COD) with increasing surfactant concentration [68].

Similar results have been obtained by A. Okada et al. [73]. These authors investigated the possible role of a particular protein, osteopontin (OPN), a major component of the kidney calcium-containing stone matrix in the crystallite morphology. To attain this goal, a comparison between wildtype and OPN knockout mice was performed.

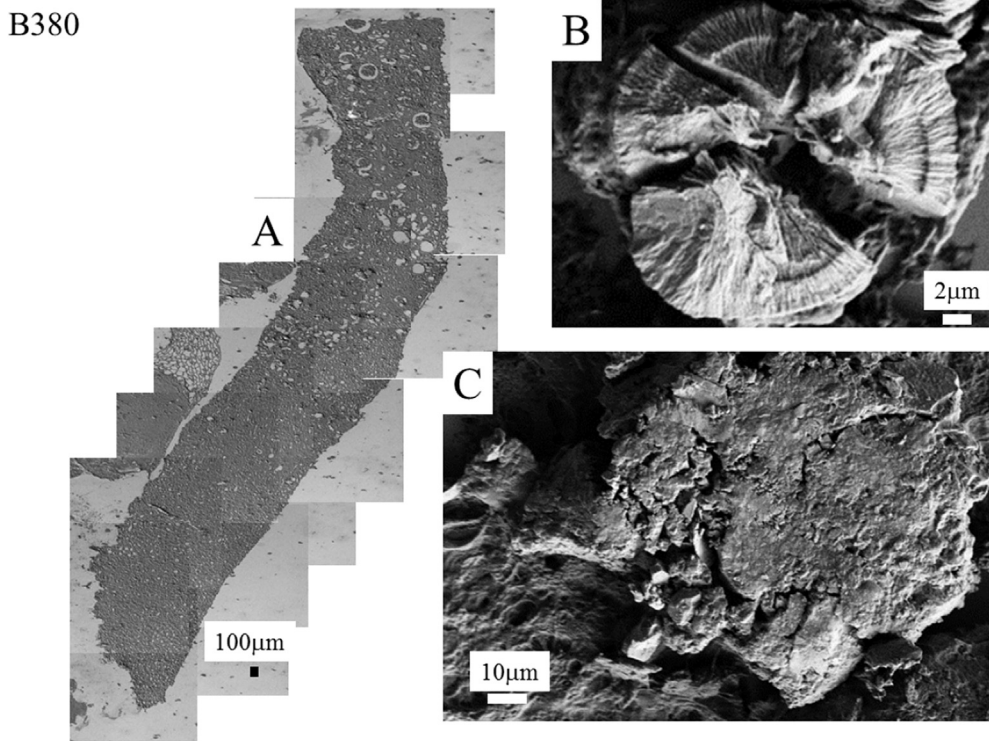


Fig. 7. A: Kidney biopsy from a patient suffering from stomach cancer (B380). Topology of the different abnormal deposits at different magnifications for the biopsy B380. B: Concentric agglomeration of platelets. C: Agglomeration of very small crystallites.

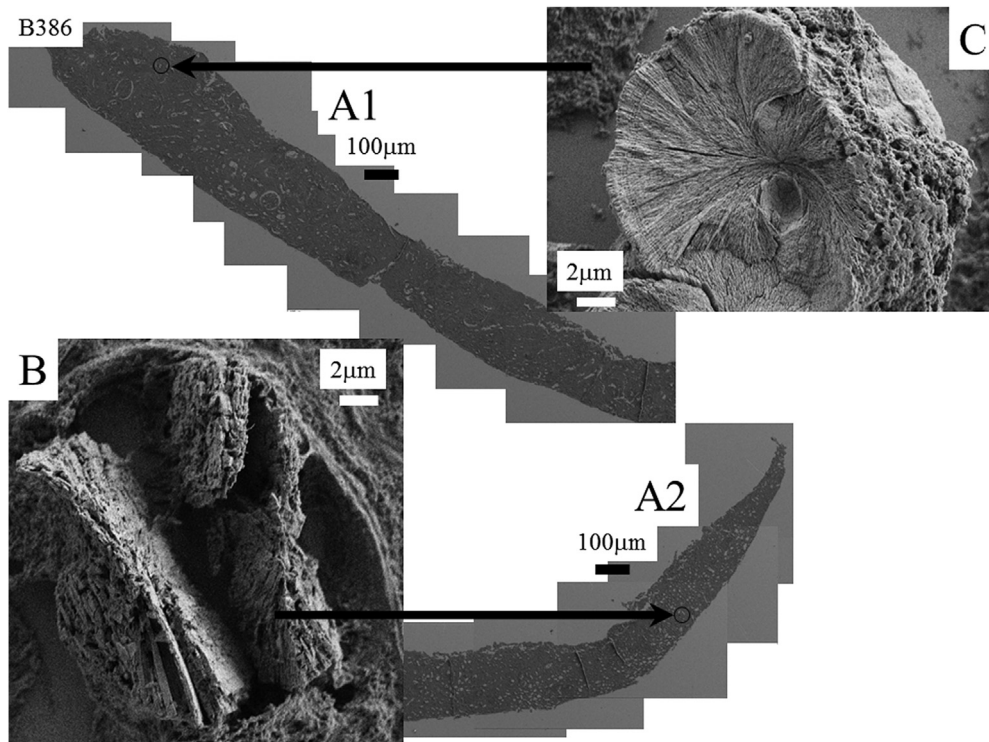


Fig. 8. A1 and A2: Nephrocalcinosis after kidney transplantation (B386). B and C: Topology of the different abnormal deposits at different magnifications for the biopsy B386. B: agglomeration of platelets C: Radial organization of platelets.

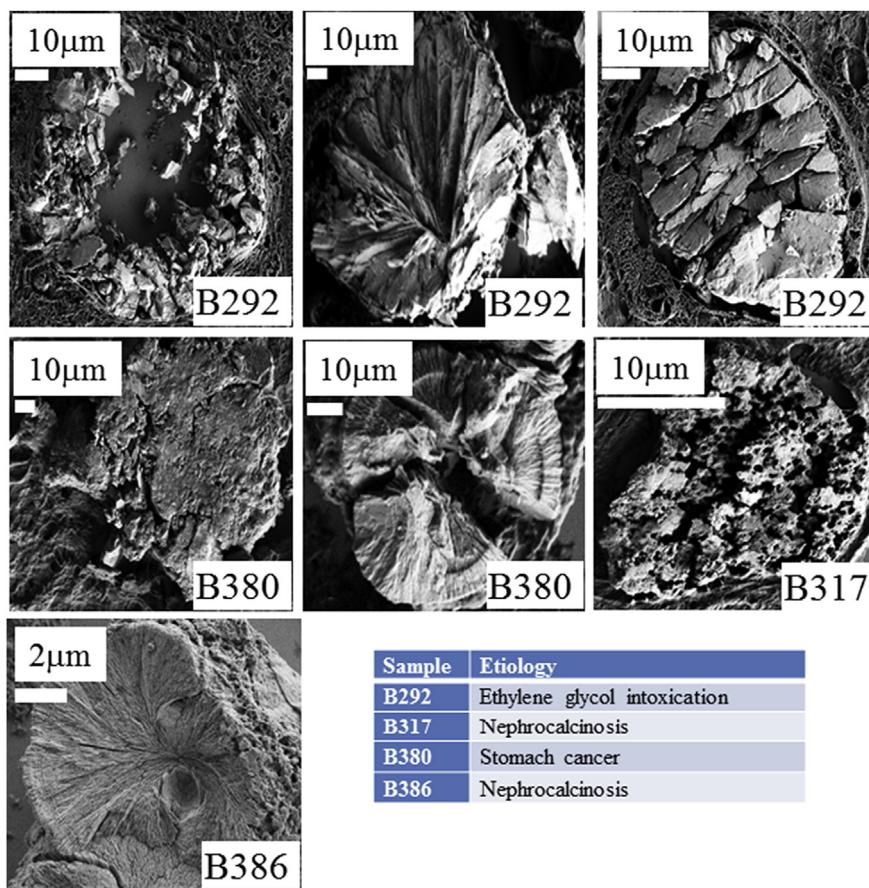


Fig. 9. Diversity of the crystallite morphologies observed for the different biopsies.

As we can see in Fig. 11, significant differences existed between large rosette and radial shaped crystals observed in WT mouse kidney (Fig. 11A) and small and uniform crystals observed in the OPN KO mouse (Fig. 11B). Thus, OPN plays a crucial role in the morphological organization of COM crystals in mouse kidneys.

These examples show that the biochemical environment of calcium oxalate crystallites plays a major role regarding their morphology. In Table 2, we have tried to gather the different morphologies pointed by FE-SEM observations.

From a physiological point of view, many kinds of ion and molecule exchange processes exist along the nephron. These exchanges imply that the biochemical environment varies significantly between the proximal tubule, the Henle's loop, the distal tubule and the collecting duct. For example, as underlined by P.S. Aronson [74], the reabsorption of NaCl in the proximal tubule occurs passively through the paracellular pathway, and actively by a transcellular route. Moreover, although short in length, the distal convoluted tubule plays a critical role in sodium, potassium, and divalent cation homeostasis [75]. These changes in the biological environment along the nephron may have a significant effect on the morphology of crystals and aggregates of calcium oxalate. If one wants to establish

a relationship between the COM crystallite morphology and the nature of hyperoxaluria, we have to combine this μ FTIR – SEM investigation with immunostaining procedures to distinguish between the different parts of the nephron.

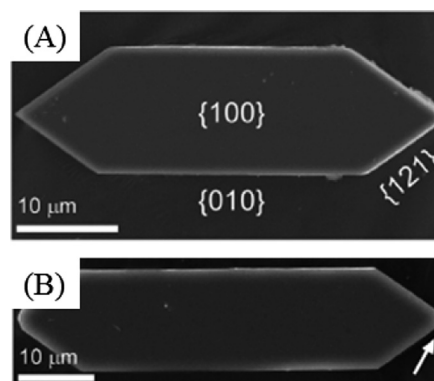


Fig. 10. (A) Control crystals exhibit an elongated hexagonal platelet morphology with basal $\{100\}$ surfaces bounded by $\{010\}$ and $\{121\}$ sides. (B) COM crystals prepared with peptide D4 exhibit a higher length-to-width aspect ratio. Several peptides in the library also induced rounding of the apical tip (arrow in B).

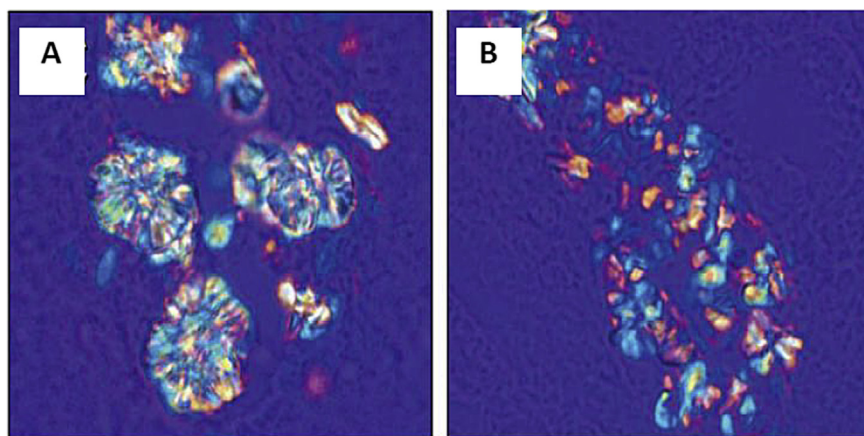


Fig. 11. Polarized light optical microscopy showed large rosette and radial shaped crystals in WT mouse kidney (A) and small and uniform crystals in the kidney of OPN KO mouse (B). (Adapted from [73]).

Table 2

Morphology of abnormal deposit of COM for the different kidney biopsies selected for this investigation.

Sample	Etiology	Morphology of abnormal deposit of COM
B274	Primary Hyperoxaluria	Agglomeration of platelets with radial organization of platelets
B292	Ethylene glycol	Agglomeration of “large” crystallites observed in the lumen of tubules, agglomeration of “small” crystallites located in the tubular cells and radial agglomeration of platelets.
B317	Nephrocalcinosis	Loose agglomerate of small crystallites
B379	Bariatric surgery	Agglomeration of “large” and “small” crystallites
B380	Stomach cancer	Concentric agglomeration of radial platelets or agglomeration of very small crystallites
B386	Nephrocalcinosis	Agglomeration of platelets with or without radial organization of platelets

4. Conclusion

In order to establish a possible relationship between the morphology of COM crystallite present in kidney biopsy and the nature of hyperoxaluria, a μ FTIR-SEM investigation has been performed. The complete set of data allows us to gather information for the first time on the physico-chemistry of the ectopic calcifications on a set of human biopsies. First, even in the case of hyperoxaluria, deposits made of calcium phosphate can be present. Such chemical diversity calls for a characterization through physico-chemical techniques like FTIR microspectroscopy for a more accurate diagnosis of the factors involved in crystallization. Moreover, even if the number of kidney biopsies included in this series is low, we have shown a diversity in the crystallite morphology, even for the very same biopsy. Various factors may be involved in such diversity including the precise location of the crystals, the presence of compounds able to modulate crystallization, and likely the composition of the fluid in the tubule depending on the segment of the nephron where the crystals are found. Further studies combining μ FTIR-SEM investigation and

immunostainings specific for the different segments of the nephron would allow one to analyze more thoroughly intratubular calcifications topography. Finally, we would like to underline that there is an opportunity to characterize the proteins present on the surface of COM nanocrystals through nano-FTIR [76–78].

Acknowledgments

This work was supported by the Physics and Chemistry Institutes of Centre National de la Recherche Scientifique and by contracts ANR-09-BLAN-0120-02, ANR-12-BS08-0022, ANR13JSV10010-01, convergence University Pierre et Marie Curie CVG1205 and CORDDIM-2013-COD130042.

References

- [1] G. Karaolani, S. Lionaki, D. Moris, V.-V. Palla, S. Vernadakis, *Transplant. Rev.* 28 (2014) 182.
- [2] J. Harambat, S. Fargue, J. Bacchetta, C. Acquaviva, P. Cochat, *Int. J. Nephrol.* 2011 (2011) 864580.
- [3] C.J. Danpure, P.R. Jennings, *FEBS Lett.* 201 (1986) 20.
- [4] P.E. Purdue, M.J. Lumb, M. Fox, G. Griffo, C. Hamon-Benais, S. Povey, C.J. Danpure, *Genomics* 10 (1991) 34.
- [5] D.E. Jacob, B. Grohe, M. Geßner, B.B. Beck, B. Hoppe, *PLoS One* 8 (2013) e70617.
- [6] B. Hoppe, B.B. Beck, D.S. Milliner, *Kidney Int.* 75 (2009) 1264.
- [7] E. Leumann, B. Hoppe, *J. Am. Soc. Nephrol.* 12 (2001) 1986.
- [8] P. Cochat, A. Deloraine, M. Rotily, F. Olive, I. Liponski, N. Deries, *Nephrol. Dial. Transplant.* 10 (1995) 3.
- [9] N. Rahman, R. Hitchcock, *J. Pediatr. Urol.* 6 (2010) 112.
- [10] B.N. Patel, C.M. Passman, A. Fernandez, J.R. Asplin, F.L. Coe, S.C. Kim, J.E. Lingeman, D.G. Assimos, *J. Urol.* 181 (2009) 161.
- [11] A. Allen, E. Clutterbuck, G. Maidment, E. Thompson, R. Watts, C. Pusey, *Nephrol. Dial. Transplant.* 12 (1997) 802.
- [12] M. Daudon, D. Bazin, G. André, P. Jungers, A. Cousson, P. Chevallier, E. Véron, G. Matzen, *J. Appl. Cryst.* 42 (2009) 109.
- [13] M. Daudon, P. Jungers, D. Bazin, *NEJM* 359 (2008) 100.
- [14] M. Daudon, P. Jungers, D. Bazin, *AIP Conf. Proc.* 1049 (2008) 199.
- [15] M. Daudon, H. Bouzidi, D. Bazin, *Urol. Res.* 38 (2010) 459.
- [16] D. Bazin, M. Daudon, G. André, R. Weil, E. Véron, G. Matzen, *J. Appl. Cryst.* 47 (2014) 719.
- [17] A. Dessombz, E. Letavernier, J.-P. Haymann, D. Bazin, M. Daudon, *J. Urol.* 193 (2015) 1564.
- [18] D. Bazin, M. Daudon, C. Combes, C. Rey, *Chem. Rev.* 112 (2012) 5092.
- [19] D. Bazin, J.-P. Haymann, E. Letavernier, J. Rode, M. Daudon, *Presse Méd.* 43 (2014) 135.
- [20] D. Bazin, M. Daudon, *J. Phys. D: Appl. Phys.* 45 (2012) 383001.

- [21] M. Daudon, D. Bazin, *J. Phys.: Conf. Ser.* 425 (2013) 022006.
- [22] L.F. Bonewald, S.E. Harris, J. Rosser, M.R. Dallas, S.L. Dallas, N.P. Camacho, B. Boyan, A. Boskey, *Calcif. Tissue Int.* 72 (2003) 537.
- [23] M. Sattler, R. Baker, N. Stone, C. Bessant, *Chemom. Intell. Lab. Syst.* 1075 (2011) 363.
- [24] C. Kendall, M. Isabelle, F. Bazant-Hegemark, J. Hutchings, L. Orr, J. Babrah, R. Baker, N. Stone, *Analyst* 134 (2009) 1029.
- [25] D. Bazin, M. Daudon, P. Chevallier, S. Rouzière, E. Elkaim, D. Thiaudière, B. Fayard, E. Foy, P.A. Albouy, G. André, G. Matzen, E. Véron, *Ann. Biol. Clin.* 64 (2006) 125.
- [26] V.K. Singh, P.K. Rai, *Biophys. Rev.* 6 (2014) 291.
- [27] E.V. Yusenko, K.V. Yusenko, I.V. Korolkov, A.A. Shubin, F.P. Kapsargin, A.A. Efremov, M.V. Yusenko, *Cent. Eur. J. Chem.* 11 (2013) 2107.
- [28] M.L. Giannossi, *J. X-Ray Sci. Technol.* 23 (2015) 401.
- [29] L. Estepa-Maurice, C. Hennequin, C. Marfisi, C. Bader, B. Lacour, M. Daudon, *Am. J. Clin. Pathol.* 105 (1996) 576.
- [30] N. Quy Dao, M. Daudon, *Infrared and Raman Spectra of Calculi*, Elsevier, Paris, 1997.
- [31] K.J. Mulready, D. McGoldrick, *Urol. Res.* 40 (2012) 483.
- [32] V.W. Petit, M. Réfrégiers, C. Guettier, F. Jamme, K. Sebanayakam, A. Brunelle, O. Laprèvote, P. Dumas, F. Le Naour, *Anal. Chem.* 82 (2010) 3963.
- [33] D. Bazin, M. Daudon, in: Jean Hamburger (Ed.), *Flammarion – Médecine*, 2010, pp. 75–98 et 277–280.
- [34] M. Pucetaite, S. Tamosaityte, A. Engdahl, J. Ceponkus, V. Sablinskas, P. Uvdal, *Cent. Eur. J. Chem.* 12 (2014) 44.
- [35] H.J. Gulley-Stahl, S.B. Bledsoe, A.P. Evan, A.J. Sommer, *Appl. Spectrosc.* 64 (2010) 15.
- [36] L. Estepa-Maurice, C. Hennequin, B. Lacour, M. Daudon, in: J.C. Merlin, S. Turrell, J.P. Huvenne (Eds.), *Spectroscopy of Biological Molecules*, Kluwer Academic Publishers, Dordrecht, 1995, p. 461.
- [37] F. Brisset, M. Repoux, J. Ruste, F. Grillon, F. Robaut, *Microscopie électronique à balayage et Microanalyses*, EDP Sciences, 2009, ISBN 978-2-7598-0082-7.
- [38] M. Daudon, D. Bazin, in: J.J. Talati, H.G. Tiselius, D.M. Albala, Z. Ye (Eds.), *Urolithiasis: Basic Science and Clinical Practice*, Springer, 2012.
- [39] D. Bazin, M. Daudon, *Ann. Biol. Clin.* 73 (2015) 517.
- [40] C. Conti, L. Brambilla, C. Colombo, D. Dellasega, G.D. Gatta, M. Realini, G. Zerbi, *Phys. Chem. Chem. Phys.* 12 (2010) 14560.
- [41] D. Di Tommaso, S.E. Ruiz Hernández, Z. Du, N.H. de Leeuw, *RSC Adv.* 2 (2012) 4664.
- [42] A.V. Kustov, A.A. Shevyrin, A.I. Strel'nikov, P.R. Smirnov, V.N. Trostin, *Urol. Res.* 40 (2012) 205.
- [43] H. Colas, L. Bonhomme-Coury, C. Coelho Diogo, F. Tielens, F. Babonneau, C. Gervais, D. Bazin, D. Laurencin, M.E. Smith, J.V. Hanna, M. Daudon, C. Bonhomme, *Cryst. Eng. Comm.* 15 (2013) 8840.
- [44] M. Hajir, R. Graf, W. Tremel, *Chem. Commun.* 50 (2014) 6534.
- [45] E. Weber, D. Levy, M. Ben Sasson, A.N. Fitch, B. Pokroy, *RSC Adv.* 5 (2015) 98626.
- [46] C. Conti, M. Casati, C. Colombo, E. Possenti, M. Realini, G.D. Gatta, M. Merlini, L. Brambilla, G. Zerbi, *Spectrochim. Acta, Part A* 150 (2015) 721.
- [47] A. Gehl, M. Dietzsch, M. Mondeshki, S. Bach, T. Hager, M. Panthofer, B. Barton, U. Kolb, W. Tremel, *Chem.—Eur. J.* 21 (2015) 18192.
- [48] Q.-Z. Gan, X.-Y. Sun, J.-M. Ouyang, *Mat. Sci. Eng. C* 59 (2016) 286.
- [49] S. Chaiyarit, N. Singht, V. Thongboonkerd, *Chem.-Biol. Interact.* 246 (2015) 30.
- [50] H. Shiraga, W. Min, W.J. Vandusen, M.D. Clayman, D. Miner, C. Miner, C. Terrell, J.R. Sherbotie, J.W. Foreman, C. Przysiecki, E.G. Nelson, J.R. Hoyer, *PNAS* 89 (1992) 426.
- [51] R.H. Glew, Y. Sun, B.L. Horowitz, K.N. Konstantinov, M. Barry, J.R. Fair, L. Massie, A.H. Tzamaloukas, *World J. Nephrol.* 3 (2014) 122.
- [52] J. Tian, J. Peng, W.H. Ge, J. Zhang, *Zhongguo Yi Xue Ke Xue Yuan Xue Bao* 36 (2014) 313.
- [53] H. Aydin, F. Yencilek, N. Mutlu, N. Çomunoğlu, H.H. Koyuncu, K. Sarica, *J. Urol.* 183 (2010) 759.
- [54] L. Estepa, M. Daudon, *Biospectroscopy* 3 (1997) 347.
- [55] M. Volmer, J.C.M. De Vries, H.M.J. Goldschmidt, *Clin. Chem.* 47 (2001) 1287.
- [56] J. Anderson, J. Dellomo, A. Sommer, A. Evan, S. Bledsoe, *Urol. Res.* 33 (2005) 213.
- [57] N.A. Channa, A.B. Ghangro, A.M. Soomro, L. Noorani, *JLUMHS* 6 (2007) 66.
- [58] J.C. Anderson, J.C. Williams Jr., A.P. Evan, K.W. Condon, A.J. Sommer, *Urol. Res.* 35 (2007) 41.
- [59] H.J. Gulley-Stahl, J.A. Haas, K.A. Schmidt, A.P. Evan, A.J. Sommer, *Appl. Spectrosc.* 63 (2009) 759.
- [60] A. Dessombz, P. Méria, D. Bazin, E. Foy, S. Rouzière, R. Weill, M. Daudon, *Prog. Urol.* 21 (2011) 940.
- [61] A. Dessombz, D. Bazin, P. Dumas, C. Sandt, J. Sule-Suso, M. Daudon, *PLoS One* 6 (2011) e28007.
- [62] F. Le Naour, C. Sandt, C. Peng, N. Trcera, F. Chiappini, A.M. Flank, C. Guettier, P. Dumas, *Anal. Chem.* 84 (2012) 10260.
- [63] M. Daudon, D. Bazin, E. Letavernier, *Urolithiasis* 43 (2015) 5.
- [64] L. Louvet, D. Bazin, J. Büchel, S. Steppa, J. Passlick-Deetjen, Z.A. Massy, *PLoS One* 10 (2015) e0115342.
- [65] J. Tonannavar, G. Deshpande, J. Yenagi, S.B. Patil, N.A. Patil, B.G. Mulimani, *Spectrochim. Acta, Part A* 154 (2016) 20.
- [66] L.M. Miller, P. Dumas, *Biochim. Biophys. Acta* 1758 (2006) 846.
- [67] L.M. Miller, P. Dumas, *Curr. Opin. Struct. Biol.* 20 (2010) 649.
- [68] X. Wei, J. Yang, Z. Li, Y. Su, D. Wang, *Colloids Surf. A: Physicochem. Eng. Aspects* 401 (2012) 107.
- [69] S. Li, W. Zhang, L. Wang, *Crys. Growth Des.* 15 (2015) 3038.
- [70] F. Grases, R.M. Prieto, R.A. Fernandez-Cabot, A. Costa-Bauza, F. Tur, J.J. Torres, *Oxid. Med. Cell. Longevity* 2015 (2015). ID 813737.
- [71] S.Y. Li, S.S. Wu, D.F. Nan, W.J. Zhang, L.J. Wang, *Chem. Mater.* 26 (2014) 5605.
- [72] S. Farmanesh, J. Chung, D. Chandra, R.D. Sosa, P. Karande, J.D. Rimer, *J. Cryst. Growth* 373 (2013) 13.
- [73] A. Okada, S. Nomura, Y. Saeki, Y. Higashibata, S. Hamamoto, M. Hirose, Y. Itoh, T. Yasui, K. Tozawa, K. Kohri, *J. Bone Miner. Res.* 23 (2008) 1629.
- [74] P.S. Aronson, *Kidney Int.* 49 (1996) 1665.
- [75] A.R. Subramanya, D.H. Ellison, *Clin. J. Am. Soc. Nephrol.* 9 (2014) 2147.
- [76] A. Dazzi, C.B. Pratter, Q. Hu, D.B. Chase, J.F. Rabolt, C. Marcott, *Appl. Spectrosc.* 66 (2012) 1365.
- [77] C. Policar, J.B. Waern, M.A. Plamont, S. Clède, C. Mayet, R. Prazeres, J.-M. Ortega, A. Vessières, A. Dazzi, *Angew. Chem., Int. Ed.* 50 (2010) 860.
- [78] A. Dazzi, R. Prazeres, F. Glotin, J.-M. Ortega, M. Alsawafah, M. de Frutos, *Ultramicroscopy* 108 (2008) 635.